Phonon-Assisted Intertube Electronic Transport in an Armchair Carbon Nanotube Film

Davoud Adinehloo[ ],[1] Weilu Gao[ ],[2] Ali Mojibpour,[3] Junichiro Kono,[3,4,5,6] and Vasili Perebeinos[ ][1]

[1]*Department of Electrical Engineering, University at Buffalo, Buffalo, New York 14228, USA*
[2]*Department of Electrical and Computer Engineering, University of Utah, Salt Lake City, Utah 84112, USA*
[3]*Department of Electrical and Computer Engineering, Rice University, Houston, Texas 77005, USA*
[4]*Department of Physics and Astronomy, Rice University, Houston, Texas 77005, USA*
[5]*Department of Materials Science and NanoEngineering, Rice University, Houston, Texas 77005, USA*
[6]*The Smalley-Curl Institute, Rice University, Houston, Texas 77005, USA*

The electrical conductivity of a macroscopic assembly of nanomaterials is determined through a complex interplay of electronic transport within and between constituent nano-objects. Phonons play dual roles in this situation: their increased populations tend to reduce the conductivity via electron scattering, while they can boost the conductivity by assisting electrons to propagate through the potential-energy landscape. We identified a phonon-assisted coherent electron transport process between neighboring nanotubes in temperature-dependent conductivity measurements on a macroscopic film of armchair single-wall carbon nanotubes. Through atomistic modeling of electronic states and calculations of both electronic and phonon-assisted junction conductances, we conclude that phonon-assisted conductance is the dominant mechanism for observed high-temperature transport in armchair carbon nanotubes. The unambiguous manifestation of coherent intertube dynamics proves a single-chirality armchair nanotube film to be a unique macroscopic solid-state ensemble of nano-objects promising for the development of room-temperature coherent electronic devices.

Toward large-scale applications of nanomaterials in electronics [1–4], understanding and controlling electron transport processes, not only within each nano-object but also between them, is crucial [5]. The overall electrical conductivity of a macroscopic assembly of nanomaterials is determined by an array of interdependent quantities, e.g., defect density, doping level, Fermi energy, material size, the density of nano-objects, purity, homogeneity, morphology, and temperature. The role of phonons in this highly complex situation is subtle, since they tend to scatter electrons to reduce the conductivity, while simultaneously assisting electrons to go through the potential-energy landscape to increase the conductivity. This dual role of phonons in electronic transport across macro-objects has not been elucidated. Particularly, phonon-assisted processes, including phonon-assisted coherent electron transfer between nano-objects, have not been identified in a macroscopic sample.

Here, we study macroscopic assemblies of carbon nanotubes (CNTs), which provide an ideal model system in which to address the above issues and questions. Since their discovery in the early 1990s [6–8], extensive studies have revealed and established the truly unique electronic and optical properties of these one-dimensional nano-objects, particularly on individual nanotube levels. Depending on the precise atomic arrangements of sp^2-bonded carbon atoms in the honeycomb lattice, specified by a pair of integers called chirality indices (n, m), both metallic and semiconducting species of CNTs exist; details of the band structure, most importantly the band gap, are determined by (n, m) [9–13]. Intertube electronic transport has also been studied theoretically [14–17] and experimentally [18–20]. Based on the momentum-matching conditions on the initial and final states of electrons in a transfer between two individual CNTs with a crossing angle θ [see Fig. 1(a)], the existence of special values of θ, where the intertube conductance becomes maximum and minimum has been identified [14–16]. We show that after structural relaxation in a CNT- crossing geometry, the overall junction conductance increases by an order of magnitude with a quantitatively similar crossing angle dependence. Moreover, following Ref. [21] for twisted bilayer phonon-assisted junction conductance, we demonstrate here that the chirality of CNTs plays a crucial role in intertube phonon-assisted junction conductance. In armchair CNTs, at room temperature, phonon-assisted junction conductance is comparable to the pure electronic conductance. At some crossing angles, phonon-assisted junction conductance of armchair CNTs exceeds its electronic counterpart by an order of magnitude. These two effects—geometry relaxation and the additional phonon-assisted mechanism—enable us to achieve better quantitative agreement with prior experiments [18] as well as the data reported here.
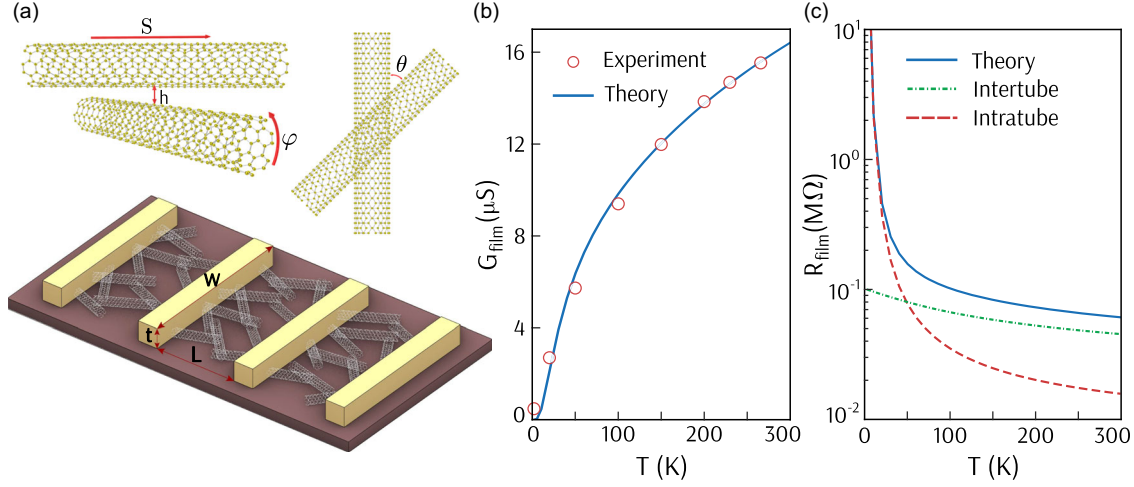
FIG. 1. (a) Schematic illustration of the device used in this Letter. The channel with length L, width W, and thickness t. θ, crossing angle; φ, rotation angle; h, interlayer distance; and S, sliding shift between CNTs. (b) Experimentally measured (red circles) and theoretically calculated (blue solid) film conductance of the (6,6) CNT film as a function of temperature. (c) Theoretically obtained total resistance of the film (blue solid) and decomposed contributions: intratube (red dashed) and a sum of the two electronic and phonon-assisted contributions to the intertube junction resistance (green dotted dashed). The calculations were performed at applied bias across the junction of $V = 1$ mV.

In our previous work [22], we investigated the temperature dependence of conductivity in a set of macroscopic single-chirality CNT films with well-defined (n, m). Distinctly (n, m)-dependent and strongly temperature-dependent conductivity was observed, and the overall behaviors were explained through the Mott variable range hopping (VRH) model in a wide temperature range. However, one of the samples—an armchair (6,6) CNT film—exhibited clear deviation from the VRH behavior, especially at elevated temperatures, indicating that a different transport mechanism was at work. Through detailed quantitative analysis of the temperature-dependent conductivity, we found that the localization length was longer in (6,6) CNT film than in the other chirality samples such that intertube transport, as opposed to intratube transport, dominated in the (6,6) film at high temperatures.

The device we used in this Letter was based on a thin film of randomly oriented chirality-enriched (6,6) CNTs as shown in Fig. 1(a). The monotonic sublinear increase of channel conductance with temperature is shown in Fig. 1(b). Through modeling and calculations of electronic and phonon-assisted junction conductance, we unambiguously identified phonon-assisted conduction as the dominant mechanism for the strong temperature dependence of the conductance observed at high temperatures, as demonstrated in Fig. 1(c). The clear manifestation of this coherent dynamic process makes a single-chirality armchair CNT film a unique macroscopic object in which to study quantum transport processes at room temperature.

The device had four electrodes and the channel between the two inner electrodes had a length L, width W, and thickness t of 8 μm, 5 μm, and 12 nm, respectively, as

shown in Fig. 1(a). Further experimental details are fully described in Ref. [22]. To understand the observed temperature dependence of the film conductance in Fig. 1(b), we consider a series resistance model of the CNT conductivity and junction resistance, which contribute to the overall resistance of the film as [23]

$$G_{\text{film}}^{-1} = C \left(\frac{L_{\text{cnt}}}{\sigma_{\text{intra}}} + \frac{1}{G_{\text{inter}}} \right), \tag{1}$$

where the first and second terms originate from the intratube conductivity σ_{intra} and the intertube junction conductance G_{inter}, respectively. A geometric prefactor C is determined by the average number of junctions in the film and is used as a fitting parameter with the best fit value $C = 0.084$ in Fig. 1(b). The calculations of network transport models have been discussed in Refs. [23–25]. In Supplemental Material [26], we developed a model for parameter $C = Lm_{\text{cnt}}/[tWnL_{\text{CNT}}^2\cos^2(\theta)]$, which depends on the carbon atom density in the sample n, mass of a CNT m_{cnt}, the average length of CNTs $L_{\text{cnt}} \approx 200$ nm, and the average angle between CNTs θ.

A temperature-dependent film conductance can arise from various sources. Our previous study on single-chirality CNT films [22] has shown that VRH is the dominant mechanism at low temperatures. Therefore, we model σ_{intra} by the 1D Mott VRH model [22], i.e., $\sigma_{\text{intra}} = \sigma_0 \exp[-(T_0/T)^{1/2}]$.

The intertube (junction) conductance G_{inter} originates from the electronic orbitals overlap on neighboring CNTs and can have a pure electronic (temperature independent) and a phonon-assistant (temperature dependent) tunneling

mechanisms. Both mechanisms depend sensitively on the distance between carbon atoms in the junction. We relaxed the atomic positions at the junction using an atomistic valence force model [31] for the internal distortions in each CNT and the Lennard-Jones potential [32] for atoms on adjacent CNTs using the Broyden-Fletcher-Goldfarb-Shanno algorithm of the quasi-Newton method [34].

In Fig. 1(b), the theory curve according to Eq. (1) includes the electronic and phonon-assistant contributions to the intertube (junction) conductance (discussed below) as well as the intratube conductivity. Since the sample is randomly oriented and the junction conductance depends on the angle θ [see Fig. 1(a)], we averaged the intertube junction conductance over a uniform angle distribution from 20° to 160° to avoid contributions from small angles. The relative contributions of the intratube and intertube resistances are shown in Fig. 1(c). At temperatures below 50 K, the intratube resistance dominates, whereas, at temperatures above 50 K, the intertube junction resistance gives a dominant contribution to the film resistance.

In the following, we discuss calculations of the intertube junction conductance. In the case of an ideally transparent contact, the maximum intertube conductance equals $4e^2/h \approx 155$ μS. However, an experimentally measured conductance [18] is substantially smaller; therefore, we use perturbation theory to calculate the intertube junction conductance as a sum of two parallel channels: electronic conductance $G_{\mathrm{inter,el}}$ due to the overlap of π orbitals on neighboring tubes described by the tight-binding model and phonon-assistant conductance $G_{\mathrm{inter,ph}}$.

Electronic intertube junction conductance.—The electronic conductance can be evaluated by [35]

$$G_{\mathrm{inter,el}} = \frac{4\pi e}{\hbar V} \sum_{\mathbf{k}ss'} M_{\mathbf{k}s}^{s'}[f(E_{\mathbf{k}s}) - f(E_{\mathbf{k}s'} + eV)], \quad (2)$$

where the spin degeneracy is included. Here, $\mathbf{k}$ is the 2D electron wave vector in 2D Brillouin zone corresponding to periodically repeated supercell containing a single junction. $s(s')$ labels the band index, e, $\hbar$, V, and f are the elementary electronic charge, the reduced Plank constant, the applied voltage bias between layers, and the Fermi-Dirac distribution function, respectively. The intertube coupling $M_{\mathbf{k}s}^{s'}$ is given by

$$M_{\mathbf{k}s}^{s'} = |\langle \psi_{\mathbf{k}s}|H_{\mathrm{el}}|\psi_{\mathbf{k}s'}\rangle|^2 \delta(E_{\mathbf{k}s'} - E_{\mathbf{k}s}), \quad (3)$$

where $\langle \psi_{\mathbf{k}s}|H_{el}|\psi_{\mathbf{k}s'}\rangle$ is the tunneling matrix element for carrier scattering from state $\psi_{\mathbf{k}s}$ to state $\psi_{\mathbf{k}s'}$ on different CNTs. $E_{\mathbf{k}s}$ is the carrier energy, calculated by the tight-binding method with the first nearest-neighbor hopping $t = 3.1$ eV. H_{el} is the electron intertube interaction Hamiltonian due to the hopping between atoms on different CNTs. The hopping parameter is defined as [36]

$$t_{ij} = t_{\perp} \exp\left(-\frac{r_{ij} - h_0}{\lambda_z}\right) \exp\left[-\left(\frac{\xi_{ij}}{\lambda_{xy}}\right)^{\alpha}\right], \quad (4)$$

where $h_0 = 3.35$ Å is the equilibrium interlayer distance, r_{ij} is the distance between atoms i and j, $\lambda_z = 0.6$ Å, $\lambda_{xy} = 1.7$ Å, $\alpha = 2.0$, and $t_{\perp} = 0.4$ eV. $\boldsymbol{\xi}_{ij}$ is the projection of $\mathbf{r}_{ij}$ onto the layers' bisector, and its absolute value is given by

$$\xi_{ij} = r_{ij} \sin\phi = r_{ij}\sqrt{1 - \left(\frac{\boldsymbol{\pi}_{ij} \cdot \mathbf{r}_{ij}}{\pi_{ij} r_{ij}}\right)^2}. \quad (5)$$

ϕ is the angle between $\mathbf{r}_{ij}$ and $\boldsymbol{\pi}_{ij}$, $\boldsymbol{\pi}_{ij} = \boldsymbol{\pi}_i - \boldsymbol{\pi}_j$, where $\boldsymbol{\pi}_i$ is determined by [31]

$$\boldsymbol{\pi}_i = 3\frac{\mathbf{r}_{ij} \times \mathbf{r}_{ik} + \mathbf{r}_{ik} \times \mathbf{r}_{il} + \mathbf{r}_{il} \times \mathbf{r}_{ij}}{r_{ij}r_{ik} + r_{ik}r_{il} + r_{il}r_{ij}}, \quad (6)$$

where j, k, and l are the three nearest neighbors of i. $\boldsymbol{\pi}_i$ is perpendicular to the surface of the CNT, and its direction points toward the outside of CNT, and $\boldsymbol{\xi}_{ij}$ is perpendicular to $\boldsymbol{\pi}_{ij}$.

Phonon-assisted intertube junction conductance.—The phonon-assisted conductance is computed by [21]

$$G_{\mathrm{inter,ph}} = \frac{4\pi e}{\hbar V} \sum_{\mathbf{k},\mathbf{k}',s,s',\mu} M_{\mathbf{k}'s'\mu}^{\mathbf{k}s}[f(E_{\mathbf{k}s}) - f(E_{\mathbf{k}'s'} + eV)]. \quad (7)$$

Here, $M_{\mathbf{k}'s'\mu}^{\mathbf{k}s}$ is given by

$$M_{\mathbf{k}'s'\mu}^{\mathbf{k}s} = |\langle \psi_{\mathbf{k}s}|H_{e\text{-ph}}^{\mu}|\psi_{\mathbf{k}'s'}\rangle|^2 [n_{\mathbf{q}\mu}\delta(E_{\mathbf{k}'s'} - E_{\mathbf{k}s} + \hbar\omega_{\mathbf{q}\mu})$$
$$\times (1 + n_{-\mathbf{q}\mu})\delta(E_{\mathbf{k}'s'} - E_{\mathbf{k}s} - \hbar\omega_{-\mathbf{q}\mu})], \quad (9)$$

where n is the Bose-Einstein function, $\langle \psi_{\mathbf{k}s}|H_{e\text{-ph}}^{\mu}|\psi_{\mathbf{k}'s'}\rangle$ is the electron-phonon matrix element, and $\omega_{\mathbf{q}\mu}$ is the phonon frequency with wave vector $\mathbf{q} = \mathbf{k} - \mathbf{k}'$ and branch number μ. The electron-phonon Hamiltonian are extracted by expanding Eq. (4) in atomic displacements corresponding to the phonon normal modes.

Since the distance between π orbitals in neighboring CNTs determines the hopping overlap, intertube junction conductance varies with the CNT structure registry. Atomic positions in an unrelaxed structure depend on the crossing angle (θ), rotation angle (φ), and sliding shift (S) between adjacent CNTs; see Fig. 1(a). In Fig. 2(a) we show $G_{\mathrm{inter,el}}$ for an unrelaxed structure versus crossing angle θ in different armchair CNTs, including (6,6) CNTs; $G_{\mathrm{inter,el}}$ can vary by more than 2 orders of magnitude as θ changes. Figures 2(b)–2(d) show that $G_{\mathrm{inter,el}}$ varies with φ and S by about 30% in (6,6) CNTs. Figure 2(b) is a surface map of $G_{\mathrm{inter,el}}$ versus φ and S with $\theta = 70°$, while Figs. 2(c) and 2(d) are detailed φ and S dependences of $G_{\mathrm{inter,el}}$,
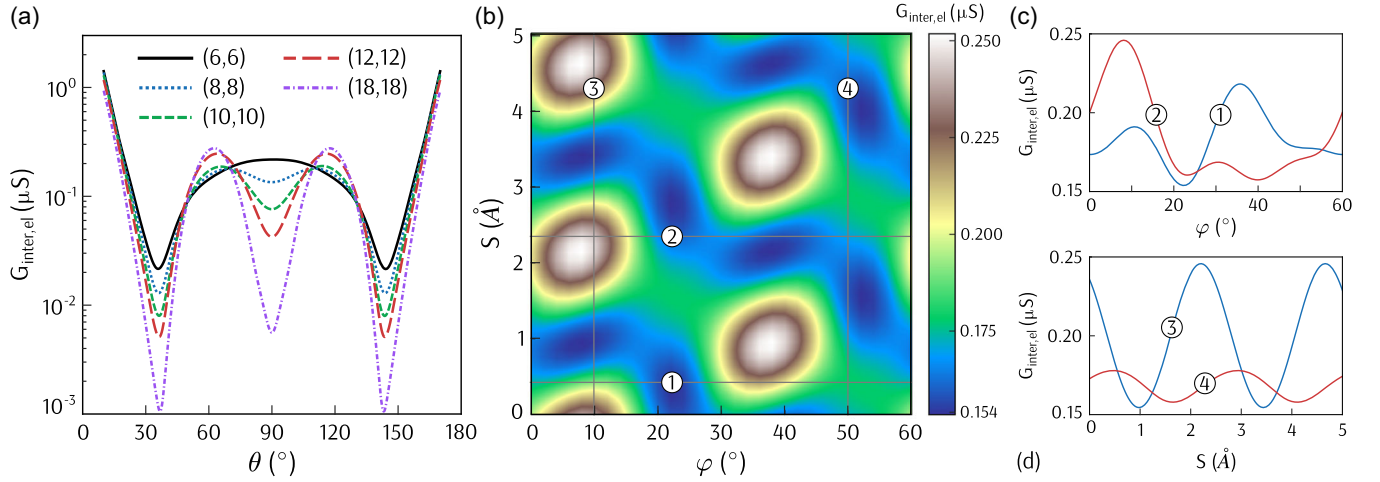
FIG. 2.   (a) Electronic conductance $G_{\mathrm{inter,el}}$ of crossed CNTs as a function of the crossing angle θ between armchair CNTs of different diameters. (b) Surface plot of $G_{\mathrm{inter,el}}$ versus S and φ in CNTs. $G_{\mathrm{inter,el}}$ versus φ in (c) and versus S in (d) at horizontal and vertical cuts depicted in (b). In (b)–(d), we used $\theta = 70°$ and (6,6) CNTs. All results were calculated at room temperature, $E_F = 0$ eV, and $V = 1$ mV.

corresponding to the labeled solid lines (1–4) in Fig. 2(b). The variation of $G_{\mathrm{inter,el}}$ with φ and S are periodic with periods of 60° and 2.46 Å, respectively, and hence, $G_{\mathrm{inter,el}}$ in Fig. 2(a) was obtained as an average over φ and S.

The large-diameter limit of G_{inter} can be understood by considering the junction conductance between twisted graphene bilayers [16], where the momentum conservation law of electrons in two Brillouin zones twisted with respect to each other by angle θ governs the tunneling probability. However, in smaller-diameter CNTs, finite curvature plays an important role such that the finite contact area between the CNTs breaks the translation symmetry and helps relax the momentum conservation requirement. As a result, the conductance variations with angles diminish in magnitude,

and a local minimum at 90° vanishes in small-diameter armchair CNTs, as shown in Fig. 2(a).

The $G_{\mathrm{inter,el}}$ of the relaxed structure is increased by an order of magnitude compared to the unrelaxed case; this arises from the fact that more atoms on neighboring CNTs get closer due to CNT bending in the contact area. Figure 3(a) depicts the $G_{\mathrm{inter,el}}$ and $G_{\mathrm{inter,ph}}$ of the relaxed structure of (6,6) CNTs versus θ, showing that overall they are comparable in magnitude at room temperature. The θ dependence of $G_{\mathrm{inter,ph}}$ is weaker than that of $G_{\mathrm{inter,el}}$ because phonons help relax the momentum conservation law. Figure 3(b) unveils the $G_{\mathrm{inter,ph}}$ and $G_{\mathrm{inter,el}}$ of relaxed (7,4) CNTs as a function of θ. As it is seen, the $G_{\mathrm{inter,ph}}$, at all angles, is smaller than $G_{\mathrm{inter,el}}$. The modest value of
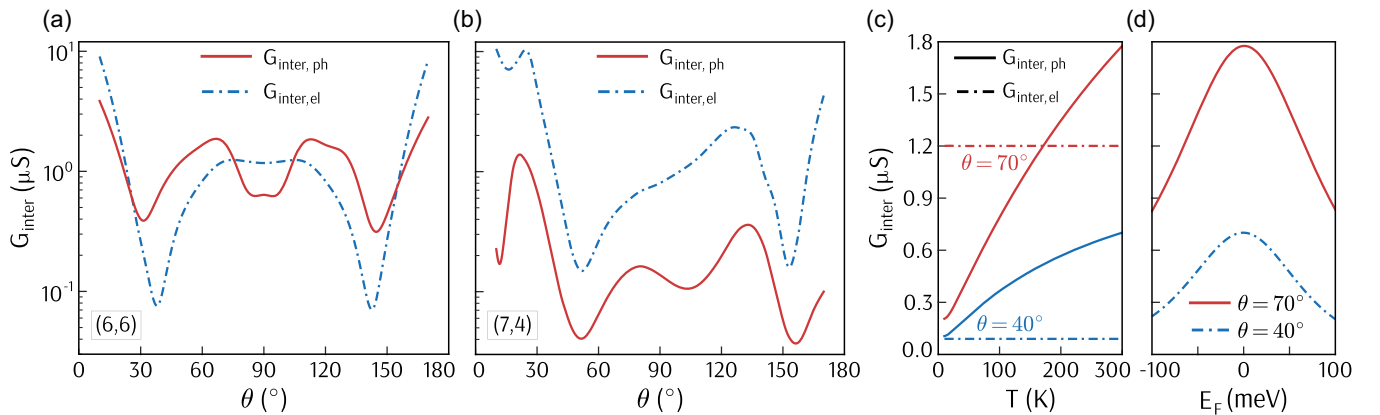

FIG. 3.   Electronic (dashed blue) and phonon-assisted (solid red) intertube junction conductance of relaxed (a) (6,6) CNTs and (b) (7,4) CNTs as a function of θ at room temperature. (c) Electronic (dashed) and phonon-assisted (solid) intertube junction conductance of crossed (6,6) CNTs for $\theta = 40°$ (blue) and $\theta = 70°$ (red). (d) Shows phonon-assisted intertube junction conductance of crossed (6,6) CNTs as a function of Fermi energy for $\theta = 40°$ (dashed blue) and $\theta = 70°$ (solid red). We used a bias of $V = 1$ mV in all panels and zero Fermi energy in panels (a)–(c).

$G_{\text{inter,ph}}$ unfolds that the temperature-dependent conductance of chiral CNTs do not eventuate from the phonons which is consistent with our previous results [22]. The small value of $G_{\text{inter,ph}}$ comes from the fact that chiral CNTs demand larger momentum to relax the momentum conservation law, see Supplemental Material [26] for the results and further details. The symmetry of conductance around $\theta = 90°$ in chiral CNTs breaks due to the momentum mismatch [16]. Note that S and φ are fixed in the relaxed structure, and there is no need to average the conductance over them.

The temperature dependence of phonon-assisted conductance $G_{\text{inter,ph}}$ is nearly linear in Fig. 3(c), reflecting the fact that low energy phonons are responsible for the phonon-assisted conductance, while the electronic intertube conductance is independent of temperature, see Supplemental Material [26]. The crossover temperature at which the two contributions become equal depends on the crossing angle. At angles near $\theta \sim 40°$, the phonon-assisted contribution dominates the intertube conductance for almost all temperatures, whereas at $\theta \sim 90°$ the electronic contribution is larger even at room temperature.

Finally, Fig. 3(d) show the calculated Fermi energy dependence of $G_{\text{inter,ph}}$. A small variation of the $G_{\text{inter,ph}}$ with the Fermi energy in Fig. 3(d) reflects the fact that electron-phonon matrix elements have a weak momentum dependence and densities of electronic states are constant. In the case of electronic intertube conductance, we find that $G_{\text{inter,el}}$ is almost independent of the Fermi energy (not shown).

In summary, we showed that in CNT films with long localization lengths, such as a chirality-enriched (6,6) CNT film, the temperature dependence of the junction conductance explains the measurements over a wide temperature range. We evaluated temperature-independent electronic junction conductance and temperature-dependent phonon-assisted junction conductance using microscopic theory as a function of the crossing angle. The phonon-assisted junction conductance is significantly larger than the electronic intertube conductance in armchair CNTs at room temperature, which explains the experimental data over a wide temperature range. We found that structural relaxation increases the electronic conductance by an order of magnitude. The low temperature measurements on individual CNTs [18] reported a factor of three higher conductance than calculated electronic intertube conductance in this work. This could be due to the lack of CNT angle control in the experiment. Our work provides guidelines for reinterpretation and analysis of other CNT network film resistances with the interplay of CNTs intratube transport and intertube junction transport.

[1] D. Jariwala, V. K. Sangwan, L. J. Lauhon, T. J. Marks, and M. C. Hersam, Chem. Soc. Rev. **42**, 2824 (2013).

[2] H. Okimoto, T. Takenobu, K. Yanagi, Y. Miyata, H. Shimotani, H. Kataura, and Y. Iwasa, Adv. Mater. **22**, 3981 (2010).

[3] R. Rao *et al.*, ACS Nano **12**, 11756 (2018).

[4] W. Gao, N. Komatsu, L. W. Taylor, G. V. Naik, K. Yanagi, M. Pasquali, and J. Kono, J. Phys. D **53**, 063001 (2020).

[5] N. F. Zorn and J. Zaumseil, Appl. Phys. Rev. **8**, 041318 (2021).

[6] S. Iijima, Nature (London) **354**, 56 (1991).

[7] S. Iijima and T. Ichihashi, Nature (London) **363**, 603 (1993).

[8] D. S. Bethune, C. H. Kiang, M. S. de Vries, G. Gorman, R. Savoy, J. Vazquez, and R. Beyers, Nature (London) **363**, 605 (1993).

[9] *Carbon Nanotubes: Synthesis, Structure, Properties, and Applications*, edited by M. S. Dresselhaus, G. Dresselhaus, and P. Avouris, Topics in Applied Physics No. 18 (Springer, Berlin, Heidelberg, 2001).

[10] P. Avouris, Z. Chen, and V. Perebeinos, Nat. Nanotechnol. **2**, 605 (2007).

[11] P. Avouris, M. Freitag, and V. Perebeinos, Nat. Photonics **2**, 341 (2008).

[12] S. Nanot, N. A. Thompson, J.-H. Kim, X. Wang, W. D. Rice, E. H. Hároz, Y. Ganesan, C. L. Pint, and J. Kono, in *Handbook of Nanomaterials*, edited by R. Vajtai (Springer, Berlin, 2013), pp. 105–146.

[13] R. B. Weisman and J. Kono, *Optical Properties of Carbon Nanotubes: A Volume Dedicated to the Memory of Professor Mildred Dresselhaus* (World Scientific, Singapore, 2019).

[14] T. Nakanishi and T. Ando, J. Phys. Soc. Jpn. **70**, 1647 (2001).

[15] A. Buldum and J. P. Lu, Phys. Rev. B **63**, 161403(R) (2001).

[16] A. A. Maarouf and E. J. Mele, Phys. Rev. B **83**, 045402 (2011).

[17] A. Davoody, F. Karimi, M. Arnold, and I. Knezevic, J. Phys. Chem. C **120**, 16354 (2016).

[18] M. S. Fuhrer, J. Nygård, L. Shih, M. Forero, Y.-G. Yoon, H. J. Choi, J. Ihm, S. G. Louie, A. Zettl, and P. L. McEuen, Science **288**, 494 (2000).

[19] M. Fuhrer, A. K. Lim, L. Shih, U. Varadarajan, A. Zettl, and P. L. McEuen, Physica (Amsterdam) **6E**, 868 (2000).

[20] S. Paulson, A. Helser, M. B. Nardelli, R. Taylor, M. Falvo, R. Superfine, and S. Washburn, Science **290**, 1742 (2000).

[21] V. Perebeinos, J. Tersoff, and P. Avouris, Phys. Rev. Lett. **109**, 236604 (2012).

[22] W. Gao, D. Adinehloo, X. Li, A. Mojibpour, Y. Yomogida, A. Hirano, T. Tanaka, H. Kataura, M. Zheng, V. Perebeinos, and J. Kono, Carbon **183**, 774 (2021).

[23] W. Shim, Y. Kwon, S.-Y. Jeon, and W.-R. Yu, Sci. Rep. **5**, 1 (2015).

[24] T. Komori and K. Makishima, Text. Res. J. **47**, 13 (1977).

[25] S. Tripathy, B. Bose, P. P. Chakrabarti, and T. K. Bhattacharyya, IEEE Trans. Electron Devices **67**, 5676 (2020).

[26] See Supplemental Material at http://link.aps.org/supplemental/10.1103/PhysRevLett.130.176303 for an estimate of constant C in Eq. (1), which includes Refs. [23,27–30].

[27] J. K. Streit, S. M. Bachilo, S. Ghosh, C.-W. Lin, and R. B. Weisman, Nano Lett. **14**, 1530 (2014).

[28] G. Drozdov, I. Ostanin, H. Xu, Y. Wang, T. Dumitrică, A. Grebenko, A. P. Tsapenko, Y. Gladush, G. Ermolaev, V. S. Volkov *et al.*, J. Appl. Phys. **128**, 184701 (2020).

[29] J. Cao, X. Yan, J. Ding, and D. Wang, J. Phys. Condens. Matter **13**, L271 (2001).

[30] X. Blase, L. X. Benedict, E. L. Shirley, and S. G. Louie, Phys. Rev. Lett. **72**, 1878 (1994).

[31] V. Perebeinos and J. Tersoff, Phys. Rev. B **79**, 241409(R) (2009).

[32] We set the van der Waals adhesion energy to $E_a = 60$ meV per atom [33] and the interlayer graphene bilayer spacing to $h = 3.35$ Å.

[33] R. Zacharia, H. Ulbricht, and T. Hertel, Phys. Rev. B **69**, 155406 (2004).

[34] M. Avriel, *Nonlinear Programming: Analysis and Methods* (Dover Publications, Englewood Cliffs, New Jersey, 2003).

[35] S. Datta, *Quantum Transport: Atom to Transistor* (Cambridge University Press, Cambridge, England, 2005).

[36] C. Tan, D. Adinehloo, J. Hone, and V. Perebeinos, Phys. Rev. Lett. **128**, 206602 (2022).

[37] https://hdl.handle.net/10477/79221.